Autonomous Nanopropulsion

DOI: 10.1002/ange.201301643

Self-Propelled Polymer-Based Multilayer Nanorockets for Transportation and Drug Release**

*Zhiguang Wu, Yingjie Wu, Wenping He, Xiankun Lin, Jianmin Sun, and Qiang He**

There is a growing effort in the scientific community to design and fabricate versatile artificial nanomotors propelled by self-generated forces, because they have potential in the field of directed drug delivery, roving sensors, isolation and detection of targets, active biomimetic systems, and other emerging applications.[1] Inspired by the nanoscale linear biomotors (for example, kinesins), which can autonomously move in aqueous solution and are powered by spontaneous hydrolysis of biological energy units, substantial efforts towards the design of chemically powerful synthetic motors at the micro- and nanoscale have recently demonstrated the ability of converting chemical energy into autonomous motion based on a fuel solution (for example, aqueous hydrogen peroxide solution).[2–4] To explain the motion and energy transfer process in these chemically powered systems, several mechanisms, including bubble propulsion,[5] interfacial tension gradients,[6] self-electrophoresis,[7] self-diffusiophoresis,[8] osmotic propulsion,[9] ultrasound propulsion,[10] and polymerization reactions[11] were proposed.

Among diverse synthetic microengines, chemically powered tubular micromotors prepared by the rolled-up technique and template electrosynthesis have displayed a high speed and the controllable directionality of the movement compared to bimetal nanorods or Janus microsphere motors.[12,13] These rocket-like microengines are capable of the pick-up, transportation, and release of various cargoes, including polymer particles,[14] nucleic acids,[15] cancer cells,[16] and bacteria.[17] However, they still have some inherent limitations, such as complex preparation technology, difficulty of surface modification, and poor biocompatibility or biodegradability. Moreover, it is required in many cases that synthetic motors can encapsulate, transport, and release targeted substances by themselves in an easy and controllable way and have good biocompatibility and biodegradability, particularly in both biomedical and environmental fields. Therefore, it still remains a challenge to develop new fabrication methods and expand the diversity of the building components.

[*] Z. Wu, Y. Wu, W. He, Dr. X. Lin, Prof. J. Sun, Prof. Q. He
Key Lab for Microsystems and Microstructure Manufacturing
The Academy of Fundamental and Interdisciplinary Sciences
Harbin Institute of Technology, Harbin 150080 (China)
E-mail: qianghe@hit.edu.cn

[**] We thank Prof. J. B. Li and Prof. H. Möhwald for their helpful discussions. This work was supported by the National Nature Science Foundation of China (91027045 and 21103034), the 100-talent Program of HIT, and the New Century Excellent Talent Program (NCET-11-0800).

Supporting information for this article is available on the WWW under http://dx.doi.org/10.1002/anie.201301643.

Herein, we describe the successful construction of a well-defined polymer multilayer tubular nanomotor through the nanoporous template-assisted layer-by-layer (LbL) assembly. It is pointed out that the pore channels of the used nanoporous template are asymmetric so that the control of the movement directionality can be conveniently achieved. Platinum nanoparticles (Pt NPs) with a uniform size and shape are assembled within the inner surface of LbL-assembled nanotubes and catalytically decompose hydrogen peroxide (as fuel) to water and oxygen. The resulting oxygen bubbles (propulsion gas) move towards the large opening, releasing oxygen bubbles from this end and in turn pushing the nanotube along (miniaturized rocket). One advantage of our approach is that not only can the length, wall thickness, and outside and inner diameters of the resulting nanotubes be controlled at the nanoscale,[18–20] but also the wall properties can be conveniently varied by assembling the corresponding components, such as polymers,[21] nanoparticles,[22] proteins,[23] and inorganic or organic functional molecules.[24] The LbL-assembled nanostructures can thus preserve the function of various building units, and multifunctional nanostructures can then easily be obtained by assembling the corresponding functional units.[25,26] More interestingly, it has been demonstrated that the LbL-assembled multilayers are responsive to external chemical, physical, or biological stimuli. Until now, most of research has focused on the LbL-assembled multilayer nanotubes with the engineered features and functions as well as on their application in biomedical fields, but they still have not been explored as autonomous motor systems. We expect that the first demonstration of highly efficient and controllable autonomous LbL-assembled tubes provide a promising platform for the development of multifunctional nanorockets, performing drug encapsulation and release and active transportation without the need of external resources.

The tubular nanorockets were fabricated by a nanoporous template-assisted LbL assembly (Figure 1a). Briefly, two biodegradable natural polysaccharides, positively charged chitosan (CHI) and negatively charged sodium alginate (ALG), were alternatively absorbed into track-etched porous polycarbonate (PC) membranes with a thickness of about 10 μm and pore diameter of about 600 nm. After the 18 bilayers with ALG as the inner layer were obtained, preformed poly(diallyldimethylammonium chloride) (PDADMAC)-stabilized Pt NPs were subsequently assembled into the template pores. Finally, well-dispersed Pt NP-modified $(CHI/ALG)_{18}$ nanotubes can be obtained after dissolution of the PC templates in CH_2Cl_2. Both transmission electron microscopy (TEM; Figure 1b) and scanning electron microscopy images (SEM: Figure 1c) of the resulting $(CHI/ALG)_{18}$-Pt NP nanotubes show well-defined tubular struc-

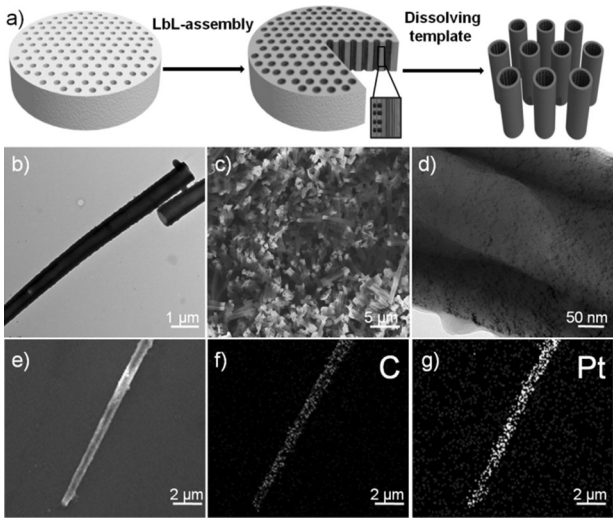

Figure 1. a) Fabrication of polyelectrolyte multilayer nanorockets. Black dots and vertical stripes (see expansion) represent Pt nanoparticles and polyelectrolyte multilayers, respectively. b),d) TEM and c) SEM images of Pt NP-functionalized $(CHI/ALG)_{18}$ nanorockets. f),g) EDX mapping analysis of a $(ALG/CHI)_{18}$-Pt NP nanorocket (e).

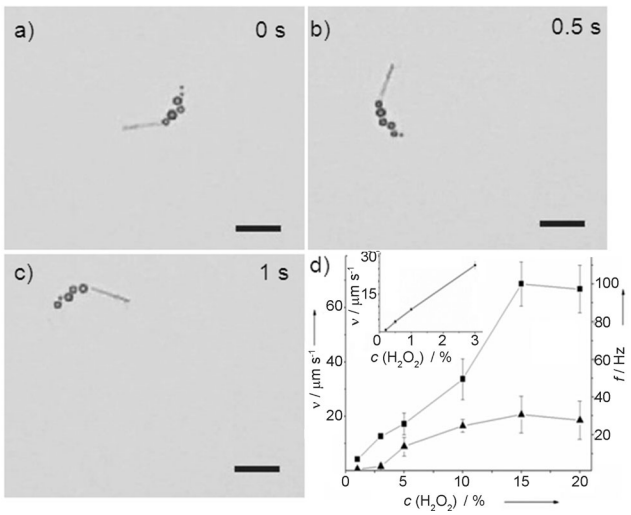

Figure 2. a)–c) Time-lapse images of the motion of a $(CHI/ALG)_{18}$-Pt NP nanorocket in 15% H_2O_2 solution recorded by using an optical microscope at 22 °C. Scale bars:10 μm. d) The dependence of the average speed v of $(CHI/ALG)_{18}$-Pt NP nanorockets (▲) and the frequency f of bubbles (■) on H_2O_2 concentration $c(H_2O_2)$ in the range of 1–20% at 22 °C. Inset: The dependence of the nanorocket speed on low H_2O_2 concentration at 37 °C.

tures with a length of 8–10 μm, in accordance with the thickness of templates. The enlarged TEM image (Figure 1 d) indicates the successful assembly of the Pt NPs with the average diameter of 5 nm into the nanotubes. Moreover, this image also verifies that the as-assembled nanotubes with the wall thickness of 140 nm exhibit an asymmetric geometry with the large-opening side of 650 ± 30 nm and relatively the small-opening side of 600 ± 10 nm. The energy-dispersive X-ray (EDX) spectrum (Supporting Information, Figure S1) clearly shows the presence of both platinum and carbon (from polyelectrolytes) and the uniform distribution of Pt NPs within the nanotubes (Figure 1 e–g).

The highly efficient propulsion power of the template-assisted LbL assembled $(CHI/ALG)_{18}$-Pt NP nanorockets is illustrated in Figure 2 (see also the Supporting Information, Videos S1, S2). Figure 2 a–c show time-lapse images taken from video (Supporting Information, Video S1), for the movement of the $(CHI/ALG)_{18}$-Pt NP nanorocket over a 1 s period at 0.5 s intervals in 15% solution at 22 °C. The oxygen bubbles are generated by the catalytic decomposition of the fuel by the Pt NPs assembled in the inner surface of the nanorockets. A tail of oxygen bubbles (ca. 4.5 μm in diameter) generated inside the nanorocket are released from the rear large-opening side of the nanorocket at a speed of 74 $\mu m\,s^{-1}$ (equal to a relative speed of nearly 10 body lengths per second). Such a speed is almost stable without obvious deceleration beyond 30 min, and the nanorocket travels distances greater than 30 cm. The drag force of the nanorocket is estimated to be 2 pN by using the Stokes's drag theory.[27] By analyzing the released oxygen bubble tails of the nanorockets, four typical trajectories, including straight, circular, curved, and self-rotating motions were found (Supporting Information, Figure S2). The diverse trajectories are apparently derived from the difference of the size and shape of the LbL assembled nanorockets as well as the distribution of catalytic Pt NPs within the nanorockets. Similar moving trajectories were previously reported for large rolled-up microengines,[28] electrosynthesized polyaniline/Pt microtubes,[29] and bacteria.[30]

As shown in Figure 2 d, the nanorockets clearly accelerate with an increase of H_2O_2 concentration over the range of 1–15% at 22 °C. The average speed increases from 5 $\mu m\,s^{-1}$ at 1% H_2O_2 to 70 $\mu m\,s^{-1}$ at 15% H_2O_2. This relationship is related to the influence of H_2O_2 concentration on the bubble frequency. In fact, the bubble frequency rises from 2 Hz to 30 Hz when the concentration of H_2O_2 was increased in the range of 1–15% (Figure 2 d). It can also be seen that a H_2O_2 concentration of over 15% has very little influence on the average speed or the bubble frequency. Furthermore (Figure 2 d, inset), the velocity of the nanorockets in the same fuel concentration increased when the solution temperature was increased from 22 to 37 °C (physiological temperature). The movement speed is 1 $\mu m\,s^{-1}$ at 0.2% H_2O_2 at 37 °C. This is ascribed to the fact that the increase of the solution temperature accelerates the rate of both mass transport and catalytic chemical reaction.[31]

Controllable locomotion of nanorockets is crucial to many applications, such as targeted delivery and the loading of targeted objects. To perform magnetic guidance of nanorockets in solution, we integrated citrate-stabilized Fe_3O_4 nanoparticles into nanorockets. As shown in the Supporting Information, Figure S3 and the corresponding video (Supporting Information, Video S3), the $(ALG/CHI)_4$-Fe_3O_4-$(CHI/ALG)_{14}$-Pt NP nanorocket navigated by an external magnetic field is able to swim along a "V"-shaped path. Although the oxidization of the Fe_3O_4 nanoparticles is not beneficial to the long-term control by the external magnetic field, this experiment has shown that to access the controlled movement of nanorockets is feasible through incorporating specific functional objects into the nanorockets.

The multilayer wall of a LbL-assembled nanotube can also be easily designed to two functional regions: the inner layers as framework and the outer layers as a container. In this case, a fluorescent anticancer drug (doxorubicin, DOX) was used to test the capability of drug encapsulation, and fluorescein isothiocyanate (FITC)-labeled CHI (FITC-CHI) to assemble the backbone of the nanorockets. Confocal laser scanning microscopy (CLSM) images (Supporting Information, Figure S4) show the successful incorporation of DOX molecules into the as-assembled $(CHI/ALG)_4$-DOX-$(ALG/CHI)_2$-Fe_3O_4-$(FITC\text{-}CHI/ALG)_{14}$-Pt NP nanorockets. A green color represents the ALG/FITC-CHI backbone (Supporting Information, Figure S4a,d), and a red color comes from the intrinsic fluorescence of DOX (Supporting Information, Figure S4e).

HeLa cells were found to survive for over 30 minutes in 3% H_2O_2 solution and did not change their shape. Figure 3 shows time-lapse images captured from video (Supporting Information, Video S4) for the motion of single $(CHI/ALG)_4$-DOX-$(ALG/CHI)_2$-Fe_3O_4-$(CHI/ALG)_{14}$-Pt NP rocket towards HeLa cells over a 6 s period at 2 s intervals in 3% H_2O_2 solution. Initially, the as-assembled nanorocket swam randomly at a speed of 22 $\mu m\,s^{-1}$ (about two body lengths per second). Under an external magnetic field, the direction of the nanorocket was navigated to approach the targeted HeLa cells. Once the rocket had attached to the HeLa cell, it did not detach from the cell, indicating that it has partially penetrated into the cell. Similarly, this targeting transport of the nanorockets could also be performed in 0.2% H_2O_2 solution at 37 °C (Supporting Information, Figure S5).

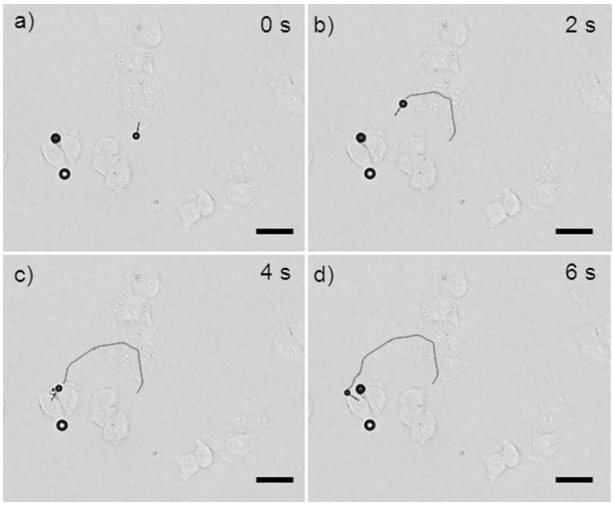

Figure 3. A time-lapse image of target location of a $(CHI/ALG)_4$-DOX-$(ALG/CHI)_2$-Fe_3O_4-$(CHI/ALG)_{14}$-Pt NP nanorocket to the HeLa cells in 3% H_2O_2 at 22 °C. The curved line shows the trajectory. Scale bars: 20 μm.

Previous studies have shown that ultrasonic treatment could trigger the breakage of the outer shell of LbL-assembled polyelectrolyte multilayer microcapsules and release the encapsulated substances.[32] Similarly, ultrasonic treatment could also be applied to perform the triggered release of the encapsulated DOX drug in the as-assembled nanorocket after it attached onto the HeLa cell. To better observe the released DOX drug on the viability of HeLa cells, two fluorescent dyes, calcein AM and propidium iodide (PI), were employed. After the LbL-assembled nanorockets bound to the HeLa cells, the sample was subjected to ultrasound at a frequency of 59 kHz and a power output of 40 W for several seconds and then HeLa cells were continually cultivated for 3 h. In a control experiment, this ultrasonic treatment did not cause any obvious adverse effects to the cell sheets.

The differential interference contrast (DIC), CLSM, SEM, and atomic force microscopy (AFM) images (Figure 4; Supporting Information, Figure S6) show the corresponding results before and after ultrasonic treatment. Both DIC (Figure 4a) and CLSM (Figure 4b) images show one $(CHI/ALG)_4$-DOX-$(ALG/CHI)_2$-Fe_3O_4-$(CHI/ALG)_{14}$-Pt NP nanorocket bound to the HeLa cells. The corresponding CLSM image (Figure 4b) reveals that the encapsulated DOX nanorockets adhered to the outer surface of the HeLa cells. Also, an SEM image (Supporting Information, Figure S5c inset) confirms that the nanorocket indeed partially penetrated into the HeLa cell. Both the SEM image (Figure 4c) and an AFM image (Supporting Information, Figure S6a) indicate that the bound nanorockets on the HeLa

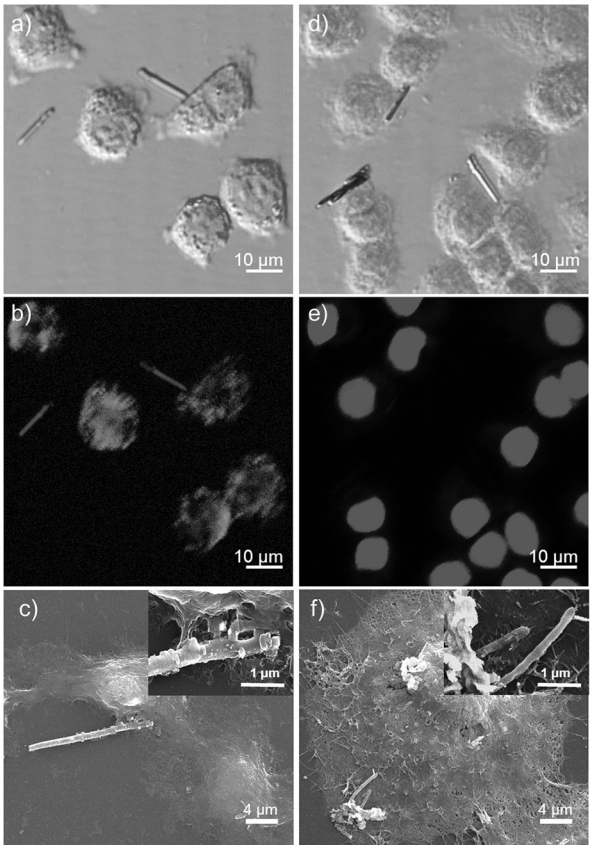

Figure 4. The DIC (a, d), the corresponding CLSM (b, e), and SEM images (c, f) of a $(CHI/ALG)_4$-DOX-$(ALG/CHI)_2$-Fe_3O_4-$(CHI/ALG)_{14}$-Pt NP nanorocket before (a–c) and after (d–f) the treatment with ultrasound in vitro and continuous cultivation of the HeLa cells for 3 h. Inset images (c, f) show the magnification of the relevant SEM images.

cells remain intact. Interestingly, a DIC image (Figure 4d) still shows a tubular structure of the as-assembled nanorockets after the ultrasonic treatment. However, in comparison to the image before ultrasonic treatment (Figure 4b), in the corresponding CLSM image (Figure 4e), the red fluorescence from the DOX in the CHI/ALG multilayer almost disappeared, showing that most of DOX molecules have been released. Actually, the SEM image in Figure 4f shows that the corresponding nanorockets are collapsed, and an AFM image (Supporting Information, Figure S6b) further confirms that the outer surface of nanorocket becomes rough and the height of the nanorockets dramatically decreased from 169 to 74 nm after the ultrasonic treatment. It suggests that the $(CHI/ALG)_{14}$-Pt NP inner layer that serves as the framework of as-assembled rocket was almost intact, but the $(CHI/ALG)_4$-DOX-$(ALG/CHI)_2$-Fe_3O_4 outer layer that serves as the drug container was broken. It should be noted that Fe_3O_4 nanoparticles play a role for the destruction of the outer multilayer shell, and its sensitivity to ultrasound depends on the volume fraction of magnetic nanoparticles.[33] Both SEM and AFM images demonstrate the breakage of the outer multilayer shell of the as-assembled nanorockets under the ultrasonic treatment, implying that the DOX drug encapsulated in the outer shell has entered into the solution around the HeLa cells. Furthermore, the released DOX from the nanorockets induced modest apoptosis of HeLa cells mainly by the inhibition of topoisomerase in nuclei and the intercalation with DNA. Although the membrane of most cells were still intact, the distinct apoptotic features of some HeLa cells are observed with calcein AM/PI staining by CLSM. The red fluorescence from the nuclei of the HeLa cells comes from the penetration of PI into the nuclei of cells from the breakage of membrane, indicating the apoptotic response of the HeLa cells after the DOX release. These results verify the feasibility of the LbL-assembled nanorockets can be used as a stimuli-response drug carrier in a biological environment.

In conclusion, we have demonstrated a versatile, simple, and cheap way to fabricate autonomous polymer multilayer nanorockets. The speed of the nanorocket motion can be tuned through changing the fuel concentration, and the motion direction can be controlled by employing an external magnetic field. Interestingly, these as-assembled nanorockets are able to be served as both autonomous motor and smart cargo, performing drug loading, targeted transportation and remote-controlled release in the vicinity of cells and tissues in an organism. Therefore, such self-propelling nanorockets may provide a novel concept to develop rapidly delivering drug carriers in future.

Received: February 26, 2013
Revised: April 8, 2013
Published online: May 23, 2013

Keywords: autonomous propulsion · drug delivery · hydrogen peroxide · layer-by-layer · nanotubes

[1] T. Mirkovic, N. S. Zacharia, G. D. Scholes, G. A. Ozin, *Small* **2010**, *6*, 159 – 167.
[2] J. Wang, *ACS Nano* **2009**, *3*, 4 – 9.
[3] G. A. Ozin, I. Manners, S. Fournier-Bidoz, A. Arsenault, *Adv. Mater.* **2005**, *17*, 3011 – 3018.
[4] Y. Hong, D. Velegol, N. Chaturvedi, A. Sen, *Phys. Chem. Chem. Phys.* **2010**, *12*, 1423 – 1435.
[5] D. A. Wilson, R. J. M. Nolte, J. C. M. V. Hest, *Nat. Chem.* **2012**, *4*, 268 – 274.
[6] W. F. Paxton, K. C. Kistler, C. C. Olmeda, A. Sen, S. K. St Angelo, Y. Cao, T. E. Mallouk, P. E. Lammert, V. H. Crespi, *J. Am. Chem. Soc.* **2004**, *126*, 13424 – 13431.
[7] R. Liu, A. Sen, *J. Am. Chem. Soc.* **2011**, *133*, 20064 – 20067.
[8] R. Golestanian, T. B. Liverpool, A. Ajdari, *New J. Phys.* **2007**, *9*, 126.
[9] U. Córdova-Figueroa, J. Brady, *Phys. Rev. Lett.* **2008**, *100*, 158303.
[10] W. Wang, L. A. Castro, M. Hoyos, T. E. Mallouk, *ACS Nano* **2012**, *6*, 6122 – 6132.
[11] R. A. Pavlick, S. Sengupta, T. McFadden, H. Zhang, A. Sen, *Angew. Chem.* **2011**, *123*, 9546 – 9549; *Angew. Chem. Int. Ed.* **2011**, *50*, 9374 – 9377.
[12] Y. Mei, G. Huang, A. A. Solovev, E. B. Ureña, I. Mönch, F. Ding, T. Reindl, R. K. Y. Fu, P. K. Chu, O. G. Schmidt, *Adv. Mater.* **2008**, *20*, 4085 – 4090.
[13] F. Kuralay, S. Sattayasamitsathit, W. Gao, A. Uygun, A. Katzenberg, J. Wang, *J. Am. Chem. Soc.* **2012**, *134*, 15217 – 15220.
[14] K. M. Manesh, M. Cardona, R. Yuan, M. Clark, D. Kagan, S. Balasubramanian, J. Wang, *ACS Nano* **2010**, *4*, 1799 – 1804.
[15] D. Kagan, S. Campuzano, S. Balasubramanian, F. Kuralay, G.-U. Flechsig, J. Wang, *Nano Lett.* **2011**, *11*, 2083 – 2087.
[16] S. Balasubramanian, D. Kagan, C. M. J. Hu, S. Campuzano, M. J. Lobo-Castañon, N. Lim, D. Y. Kang, M. Zimmerman, L. Zhang, J. Wang, *Angew. Chem.* **2011**, *123*, 4247 – 4250; *Angew. Chem. Int. Ed.* **2011**, *50*, 4161 – 4164.
[17] S. Campuzano, J. Orozco, D. Kagan, M. Guix, W. Gao, S. Sattayasamitsathit, J. C. Claussen, A. Merkoçi, J. Wang, *Nano Lett.* **2012**, *12*, 396 – 401.
[18] K. K. Chia, M. F. Rubner, R. E. Cohen, *Langmuir* **2009**, *25*, 14044 – 14052.
[19] S. Ai, G. Lu, Q. He, J. Li, *J. Am. Chem. Soc.* **2003**, *125*, 11140 – 11141.
[20] M. Steinhart, J. H. Wendorff, A. Greiner, R. B. Wehrspohn, K. Nielsch, J. Schilling, J. Choi, U. Gösele, *Science* **2002**, *296*, 1997.
[21] Y. Yang, Q. He, L. Duan, Y. Cui, J. Li, *Biomaterials* **2007**, *28*, 3083 – 3090.
[22] D. Lee, R. E. Cohen, M. F. Rubner, *Langmuir* **2007**, *23*, 123 – 128.
[23] S. Hou, J. Wang, C. R. Martin, *Nano Lett.* **2005**, *5*, 231 – 234.
[24] L. Zhang, A. Vidyasagar, J. L. Lutkenhaus, *Curr. Opin. Colloid Interface Sci.* **2012**, *17*, 114 – 121.
[25] Q. He, Y. Cui, S. Ai, Y. Tian, J. Li, *Curr. Opin. Colloid Interface Sci.* **2009**, *14*, 115 – 125.
[26] W. Qi, L. Duan, J. Li, *Soft Matter* **2011**, *7*, 1571 – 1576.
[27] W. Gao, S. Sattayasamitsathit, J. Orozco, J. Wang, *J. Am. Chem. Soc.* **2011**, *133*, 11862 – 11864.
[28] A. A. Solovev, Y. Mei, E. Bermúdez Ureña, G. Huang, O. G. Schmidt, *Small* **2009**, *5*, 1688 – 1692.
[29] W. Gao, A. Uygun, J. Wang, *J. Am. Chem. Soc.* **2012**, *134*, 897 – 900.
[30] V. B. Shenoy, D. K. Tambe, A. Prasad, J. A. Theriot, *Proc. Natl. Acad. Sci. USA* **2007**, *104*, 8229 – 8234.
[31] S. Sanchez, A. N. Ananth, V. M. Fomin, M. Viehrig, O. G. Schmidt, *J. Am. Chem. Soc.* **2011**, *133*, 14860 – 14863.
[32] A. G. Skirtach, B. G. D. Geest, A. Mamedov, A. A. Antipov, A. Kotov, G. B. Sukhorukov, *J. Mater. Chem.* **2007**, *17*, 1050 – 1054.
[33] T. Liu, H. Huang, Y. Chen, Y. Chen, *Acta Biomater.* **2011**, *7*, 578 – 584.

